Research Journal of Applied Sciences, Engineering and Technology 15(4): 132-142, 2018
DOI:10.19026/rjaset.15.5844
ISSN: 2040-7459; e-ISSN: 2040-7467

Submitted: August 4, 2017 Accepted: October 21, 2017 Published: April 15, 2018

Research Article

Design and Shape Optimisation of Nozzles for a Flat Air Bearing Device

H. Monfared, E. Eslamian and H. Shirvani
Department of Engineering and Built Environment, Anglia Ruskin University, Chelmsford, Essex, CM1 1SQ, UK

Abstract: This study offers a numerical and experimental study in the design and further shape optimisation of nozzles for a flat type air-bearing device which is supposed to be used for handling a certain magnitude of loads. Making use of pressurised air allows for the design of mechanical systems requiring handling heavy loads or extreme precision in positioning. In a design of flat type air-bearings, particularly when carrying heavy loads is considered, the shape of nozzles becomes very important. In order to analyse and further optimisation of the dimensions of a nozzle in this study, Computational Fluid Dynamic (CFD) analysis with k-ω turbulence modelling has been performed to simulate the supersonic fluid flow behaviour inside the chamber and divergent nozzle of the bearing device. Three different geometries with fixed inlet diameter of 2 mm and outlet diameters of 3, 6 and 12 mm were studied. An experimental investigation was conducted with the same nozzle geometries and also different nozzle numbers (and arrangements) to find the best option with respect to the performance in handling loads. Results from experimental study are in accordance with results of CFD analysis, making the numerical modeling a useful tool for a comparative study in this research to determine the optimum size and shape of nozzles as well as optimum pressure for a particular load.

Keywords: Air bearing, experimental study, nozzle optimisation

INTRODUCTION

Nowadays, the industrial factories are benefiting from cutting-edge technologies for handling heavy loads by interposing a fluid layer with low horizontal stiffness between the load panel and the ground. One of the most well-known technologies is the Air Bearing system, which produces a thin layer of pressurised air between the load base plane and the surface of the ground giving an advantage of a near zero friction. The fluid film of the bearing is achieved by supplying a flow of air through the bearing face and into the bearing gap. This is typically accomplished through an orifice to provide the flow of air into the gap. This kind of air bearings is known as Flat Air Bearing or Rigid Air Bearing. Unlike the cushion type bearings, there is no rubber made cushion below the device to maintain the air volume. Flat bearings maintain a finite separation between mechanical components by means of the pressurised flow of air through the gap between two surfaces. A well-known example of this kind is an air hockey table, where a puck is floated above the table surface by an array of vertical jets of air (Hendriks, 2001). Using flat air bearings there is no contact between "moving parts" and thus no friction and no wear on surfaces. Having known the geometry of the air-bearing device, the design and optimisation of the nozzles are crucial. One of the pioneer researchers in this area is Powell (1970), who published a book, namely "Design of Aerostatic Bearings" in 1970 (Powell, 1970). He introduced basic equations, which are commonly used in the modelling of the mass flow-rate of gas through an orifice-type restrictor in aerostatic bearings. In Renn and Hsiao (2004) proposed a CFD simulation focusing on the mass flow-rate characteristic of gas through an orifice, based on using empirical equations for estimation of controlling coefficients which results in some limitations in the application of the method. In Mukai (2006) investigated the dynamic properties of a manufacturer made air-bearing units. In that report, the effects of shape and geometry of the orifice or nozzle are not presented, whereas the shape of the nozzle can play a significant role in changing the capacity of the air bearing. Another research by Wei and Gang (2010) shows the effect of entrance on the load capacity of a nozzle. In their study, the density of a fluid is assumed as a constant which may not lead to accurate results in turbulence and high Mach numbers.

Corresponding Author: H. Monfared, Department of Engineering and Built Environment, Anglia Ruskin University, Chelmsford, Essex, CM1 1SQ, UK

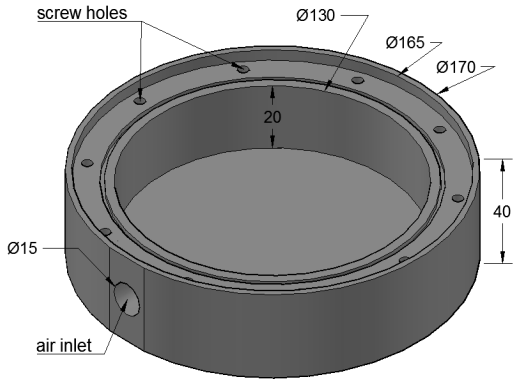

Fig.1: Body (chamber) of the air-bearing device (dimensions in mm)

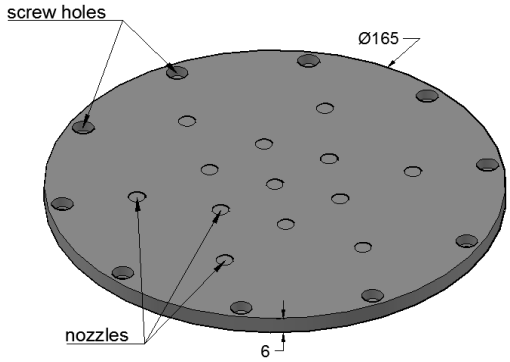

Fig. 2: Seal of the air-bearing device and the position of the nozzles (dimensions in mm)

The air-bearing device proposed in this study is a flat air bearing, which is supposed to be used for handling a part of the weight of a benchmark structure in laboratory dynamic tests.

The air-bearing device here is proposed, designed and further optimised with respect to the number of nozzles and nozzle geometry, to be able to handle a heavier load. In this particular design, the conditions of tests and availability of space under the benchmark structure determine the geometry of the air-bearing device.

PROBLEM IDENTIFICATION

There is a limited space underneath of a benchmark scaled model structure prepared and built for future laboratory dynamic tests. The air bearing solution as part of the isolation system proposed for base isolation of the benchmark, required to be designed and further optimised to handle a certain part of the total weight of the structure. There will be at least two numbers of the same device to be used in the tests. With respect to the space available in the isolation level, the geometry of every individual device is determined. The device comprises of two parts, body and seal (Fig. 1 and 2).

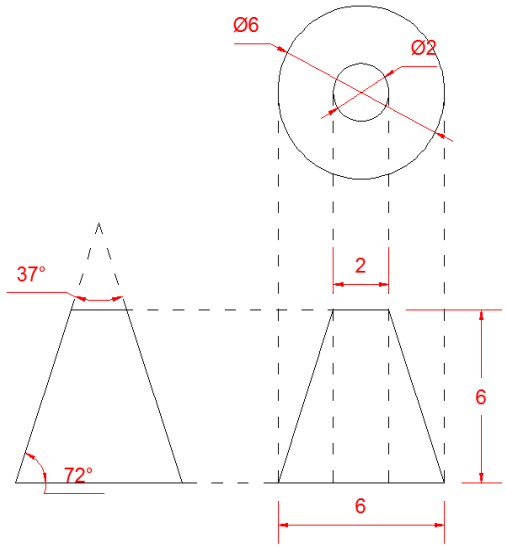

Fig.3: Typical nozzle geometry

The seal of the bearing is attached to the chamber through the designated screw holes on the wall of the chamber.

The changeable seal gives the opportunity of testing different nozzle shapes and numbers. Having known the feasible size and geometry for the bearings, it is possible to model it in a CAD software and analyse the fluid flow with respect to the maximum pressure available at the workshop. Simulations are to determine the optimum geometry for nozzles and further optimisation of the number of nozzles. The primary shape of the nozzle for this type of air bearing consists of an orifice with a cylindrical pocket. The shape considered for initial simulation is a conical shape shown in

The flow enters the nozzle from 2 mm diameter side and exits from 6 mm diameter (Fig. 3). In fact, the inlet of the nozzle is designed to have a smaller diameter than its outlet. The flow that enters the nozzle reaches Mach velocity rapidly due to high-pressure differences between inlet and outlet. As the flow becomes supersonic, the nozzle should have a divergent shape to maintain the high velocity otherwise, the flow velocity will drop to the subsonic area. The higher velocity is desired as it produces higher momentum.

In order to gain an insight into what happens to the flow inside the chamber and nozzle, it is necessary to create a computer simulation with respect to the geometry constraints and boundary conditions. The simulation also provides valuable information about the fluid characteristics such as pressure, velocity and consequently the mass flow rate. The mass flow rate can be used to validate the total momentum force generated in the nozzle. The next section will discuss the simulation method in light of the governing equations of fluid flow.

NUMERICAL STUDY

Governing equations: The governing equations of the fluid flow could be described by the problems of continuum mechanics. In continuum motion the governing equations are as follows:

$$\frac{d}{dt}\int_{V_M(t)}\rho\emptyset(\mathrm{x},t)dV = \frac{\partial}{\partial t}\int_{V_M(t)}\rho\emptyset dV + \partial VMtd\mathrm{S}.\rho\emptyset\mathrm{U}, \quad (1)$$

In Eq. (1). U is the velocity vector and *d*Sis the outward pointing unit vector normal to $\partial V_M(t)$. The rate of change of $\emptyset$ in V_M can be written with regard to its volume and surface sources:

$$\frac{\partial}{\partial t}\int_{V_M(t)}\rho\emptyset dV + \oint_{\partial V_M(t)} d\mathrm{S}.(\rho\emptyset\mathrm{U}) = \int_{V_M(t)} Q_V(\emptyset)dV + \oint_{\partial V_M(t)} d\mathrm{S}.\mathrm{Q}_S(\emptyset), \quad (2)$$

The differential form of the above is:

$$\frac{\partial\rho\emptyset}{\partial t} + \nabla.(\rho\emptyset\mathrm{U}) = Q_V(\emptyset) + \nabla.\mathrm{Q}_S(\emptyset). \quad (3)$$

Equation (3) is a governing equation for all continuum mechanics problems in general (Aris, 1989). The equation is transformed to different conservation equations by changing parameter $\emptyset$.

Conservations laws: The conservation laws valid for any continuum are as follow:

- Conservation of mass ($\emptyset$ = 1):

$$\frac{\partial\rho}{\partial t} + \nabla.(\rho\mathrm{U}) = 0 \quad (4)$$

- Conservation of linear momentum ($\emptyset$ = U):

$$\frac{\partial\rho\mathrm{U}}{\partial t} + \nabla.(\rho\mathrm{UU}) = \rho\mathrm{g} + \nabla.\sigma \quad (5)$$

- Conservation of energy ($\emptyset$ = *e*):

$$\frac{\partial\rho e}{\partial t} + \nabla.(\rho e\mathrm{U}) = \rho\mathrm{g}.\mathrm{U} + \nabla.(\sigma.\mathrm{U}) - \nabla.\mathrm{q} + \rho Q. \quad (6)$$

where,
ρ = The density
U = The velocity vector
σ = The stress tensor
e = The total specific energy
Q = The volume energy source

The system is still indeterminate as the number of unknown quantities is larger than the number of equations. There is a need to introduce additional conservative relations to increase the number of equations and close the system.

Considering the fluid as a *Newtonian* fluid, the following set of equations can be used (Jasak, 1996):

- Defining the internal energy as a function of pressure *P* and temperature *T*:

$$u = u(P,T). \quad (7)$$

- The total energy e can be defined as the sum of the kinetic energy e_k and internal energy:

$$e = e_k + u(P,T) = \frac{1}{2}\mathrm{U}.\mathrm{U} + u(P,T), \quad (8)$$

- The equation of state:

$$\rho = \rho(P,T), \quad (9)$$

- The Fourier's law of heat conduction:

$$\mathrm{q} = -\lambda\nabla T, \quad (10)$$

where,
q = The heat flux
λ = The transport coefficient

Generalised form of the Newton's law of viscosity:

$$\sigma = -\left(P + \frac{2}{3}\mu\nabla.\mathrm{U}\right)\mathrm{I} + \mu[\nabla\mathrm{U} + (\nabla\mathrm{U})^T]. \quad (11)$$

where,
μ = Viscosity
I = The unit tensor

The constitutive relations above, together with the governing equations of continuum mechanics can create a close system of partial differential equations for a *Newtonian* fluid:

Continuity equation:

$$\frac{\partial\rho}{\partial t} + \nabla.(\rho\mathrm{U}) = 0 \quad (12)$$

Navier-Stokes **(momentum) equation:**

$$\frac{\partial\rho\mathrm{U}}{\partial t} + \nabla.(\rho\mathrm{UU}) = \rho\mathrm{g} + \nabla.\left(P + \frac{2}{3}\mu\nabla.\mathrm{U}\right) + \nabla.[\mu(\nabla\mathrm{U} + (\nabla\mathrm{U})^T)], \quad (13)$$

Energy equation:

$$\frac{\partial\rho e}{\partial t} + \nabla.(\rho e\mathrm{U}) = \rho\mathrm{g}.\mathrm{U} + \nabla.(P\mathrm{U}) - \nabla.\left(\frac{2}{3}\mu(\nabla.\mathrm{U})\mathrm{U}\right) + \nabla.[\mu(\nabla\mathrm{U} + (\nabla\mathrm{U})^T).\mathrm{U}] + \nabla.(\lambda\nabla T) + \rho Q. \quad (14)$$

As functions of thermodynamics state variables, the transport coefficients λ and μ are defined as follow:

$$\lambda = \lambda(P,T), \quad (15)$$

$$\mu = \mu(P,T). \quad (16)$$

Turbulence modelling: The state of continuous instability in a flow is called turbulence. Irregularity in the flow, increased diffusivity and energy dissipations are some characters of a turbulent flow (Jasak, 1996). Several deferent approaches can be conducted in order to model a turbulent flow. The Direct Numerical Simulation or DNS is a way in which the governing equations are numerically integrated (Eswaran and Pope, 1988). The Large Eddy Simulation (LES) is another way in which a spatial filter is applied in order to separate different length scales which was first introduced by (Deardorff, 1970). Both two ways are among the pioneers in fluid turbulence numerical analysis yet demanding high computer specifications and rendering time.

An alternative approach is a separation of the local value of the variable into the mean value and the fluctuation around the mean. In this case, the characteristics of turbulent flow govern the selection of the averaging method.

Reynolds averaging technique: One of the popular techniques is *Reynolds* averaging technique in which all flow parameters are presented as mean value plus a fluctuation value as follow:

$$\emptyset(\mathrm{x},t) = \bar{\emptyset}(\mathrm{x},t) + \emptyset'(\mathrm{x},t), \quad (17)$$

where, $\emptyset'(\mathrm{x},t)$ is the fluctuation about the mean value and the mean value is defined as below:

$$\bar{\phi}(\mathrm{x},t) = \lim_{\mathrm{N}\to\infty} \frac{1}{N}\sum_{i=1}^{N} \phi_i(\mathrm{x},t), \quad (18)$$

In this equation, N is the number of identically performed experiments.

The following form of the averaged will be obtained if the above procedure is applied to the compressible *Navier-Stokes* equation:

$$\frac{\partial}{\partial t}(\rho\bar{\mathrm{U}}) + \nabla.(\rho\bar{\mathrm{U}}\bar{\mathrm{U}}) = \mathrm{g} - \nabla\bar{p} + \nabla.(\nu\nabla\bar{\mathrm{U}}) + \overline{\mathrm{U}'\mathrm{U}'}. \quad (19)$$

The term $\overline{\mathrm{U}'\mathrm{U}'}$ is called the Reynolds stress tensor. The Reynolds stress represents effects of the turbulence and has to be modelled to close the system of equations (Ramezanpour, 2009). In order to express the Reynolds stress tensor in terms of the known quantities, Reynolds averaged turbulence modelling is necessary. One of the approaches is the *Standard k-ω* which is used for modelling in this study.

Numerical solutions: As there is no analytical solution for partial differential equations governing fluid flow problems and on the other hand, the experimental study is costly and time taking for a high number of design variables, the best option to analyse and finalise the air-bearing design is using numerical methods for the solution of mathematically defined fluid flow governing equations. CFD (Computational Fluid Dynamics) analysis is employed for solving the problem of fluid flows in this study in order to determine the optimised geometry of the nozzles.

Domain geometry: CFD analysis starts with generating the geometry of the model. It should be noted, all geometry components are parametric in this model which enables the user to change them for desired dimensions. The general geometry of the air-bearing unit used in this study is shown in Fig. 4.

The geometry of CFD model is a cylinder shape volume with the diameter of 130 mm and height of 20 mm. The inlet has the length of 30 mm and diameter of 10 mm. The outlet is a nozzle to the centre of bottom plate Fig. 5.

The thickness of the bottom plate is 6mm and the material of the device is Aluminium. The air-bearing unit can lift up with producing a thin layer of air flow underneath on the bottom. The air pressure on the inlet of the unit is set to 5bars (gauge). The CFD model for this analysis is responsive when applying changes in inlet and outlet boundaries.

Domain discretisation: The problem space or the domain of the model is divided into a finite number of volumes or regions, known as control volume or mesh. The numerical solution in this study is based on finite volume method in which the integral form of the governing equations on each control volume or cell is considered. Therefore, the flow domain is subdivided into tetrahedral cells where governing equations are solved subsequently. Control volume or cells fill the whole domain volume and do not overlap. With respect to the geometry of the domain and the solution method, the discretization is carried out in unstructured cells. This kind of grids normally hires triangle shapes in two-dimensional and tetrahedral in 3D domains (Mavriplis, 1996). For this geometry, approximately, 3 million tetrahedral unstructured cells are generated with prism layer mesh at the boundaries to capture velocity gradients near the walls. There is higher mesh density inside the nozzle in order to capture shock waves and expansion fans.

Boundary conditions: The partial differential equations governing the problem need boundary conditions in order close the system of equations. The set of boundary conditions implemented are as below:

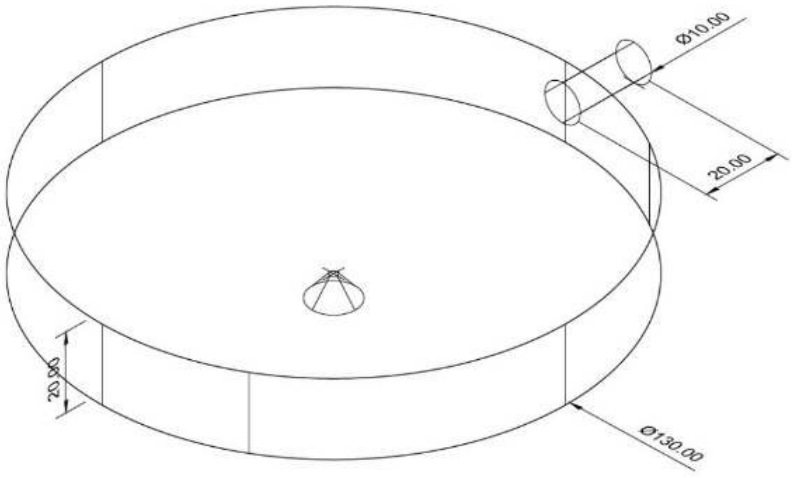

Fig.4: Domain geometry in CFD (dimensions in mm)

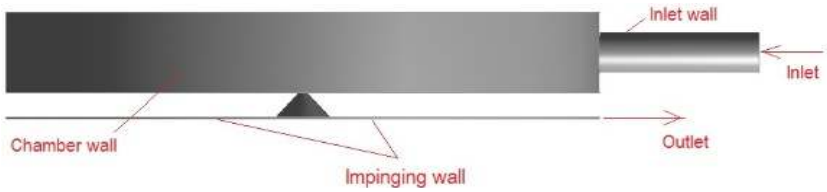

Fig.5: The geometry of flow domain

The inlet boundary condition is defined as "pressure inlet" of 5bar gauge. The flow inside the chamber and inside the nozzle is solved for different pressure ratios. The inlet pressure to the chamber is known; on the other hand, the velocity and mass flow rate are unknown. The relationship between variables in the case of compressible flow is as follows:

$$p_t = p_s(1 + \frac{\gamma-1}{2}M^2)^{\frac{\gamma}{\gamma-1}} \quad (20)$$

where,
p_t = Total pressure
p_s = The static pressure
γ = The specific heat ratio and
M = Mach number defined as below:

$$M = \frac{u}{\sqrt{\gamma R T_s}} \quad (21)$$

In the above equation, u represents the velocity, T_s is the static temperature and R denotes the gas constant. The static temperature relationship with total temperature is described as:

$$\frac{T_t}{T_s} = 1 + \frac{\gamma-1}{2}M^2 \quad (22)$$

The outlet boundary condition is defined as "pressure outlet" which is atmospheric conditions pressure of 1.013bar (zero gauge).

The solid wall boundary condition is utilised in solid regions, with no-slip conditions. In order to take into account the effect of viscosity of the flow on the solid walls, the wall boundary conditions are imposed the shear stress for laminar flows, which are calculated (based on the velocity gradient at the wall) as below:

$$\tau_w = \mu \frac{\partial u}{\partial n} \quad (23)$$

where,
τ_w = Shear stress at the wall
μ = The coefficient of friction

Equations discretisation: The partial differential equations of governing equations are expressed in the algebraic form, in terms of discrete quantities defined at each cell in the domain. Therefore, Eq. (3). Becomes:

$$a_p \emptyset_p^{t+\Delta t} = \sum_{f=1}^{nb} a_{nb} \emptyset_{nb}^{t+\Delta t} + S_K \quad (24)$$

where, a_p and a_{nb} represent the cell centre and neighbouring cell coefficient respectively. The cell centre coefficient is calculated as follow (Brennan, 2001):

$$a_p = \sum_{f=1}^{nb} a_{nb} - S_L \quad (25)$$

In Eq. (24) and (25)., S_K and S_L are dimensionless source terms in integration.

Table 1: Simulation cases

Simulation case	Inlet diameter (mm)	Outlet diameter (mm)
2-3	2	3
2-6	2	6
2-12	2	12

Solver: For this research, density base solver has been employed with implicit steady state condition for the time frame. In order to reduce the errors, a high order of discretization schemes has been used. For momentum equations, third order MUSCL scheme has been adopted and for rest of the parameters, a second order upwind method has been implemented. To avoid instabilities in the solution domain, Courant number (CFL) was set to be below one. As the simulations are carried out for compressible flow, therefore, the air has been considered as an ideal gas. The solver used for this study is the FLUENT commercial package.

NUMERICAL RESULTS

CFD model in this study is a parametric model with a capability of applying changes in all geometry parameters. The CFD was applied for three different nozzle geometries and a gap height of 1 mm between the bottom of the air-bearing device and the flat surface. In all three cases, the inlet diameter was set to 2 mm, however, the simulation was performed for three different outlet diameters (Table 1).

Mach contours analysis: In order to determine the optimum slope for a conical nozzle, the effect of velocity in nozzle should be considered. Figure 6 to 8 show the contours of Mach number in the cross-sectional area of nozzle and gap for three different nozzles. Mach number is the ratio of actual velocity over the velocity of sound which is helpful for investigating the velocity of compressible flow in a specific field and observation of shock waves.

In a flow field, the Stagnation point is a point with zero local velocity (Clancy, 1975). According to Bernoulli equation, pressure and velocity have the inverse relationship; the pressure is at its maximum level when the velocity is minimum. Therefore, in a fluid flow where the velocity is zero or near zero (stagnation point), the static pressure is maximum. This pressure is called Stagnation pressure. With reference to Fig. 6 to 8, the largest area of stagnation pressure exists in the case of a nozzle with 2 mm inlet and 6 mm outlet. The stagnation area creates a cushion of air that the air bearing stands on it. Therefore, it can produce more uplift pressure underneath of the bottom plate of the air-bearing unit.

A comparison of Mach number contour results shows that in the nozzle with 12 mm outlet diameter, there is a large separation zone on the nozzle wall. This is due to the high adverse pressure gradient that separates the flow. The circulationzone, as a result of pressure gradient, is a non-desirable phenomenon as it blocks the air flow. Although the maximum velocity is not happening in the nozzle 2-6, due to larger

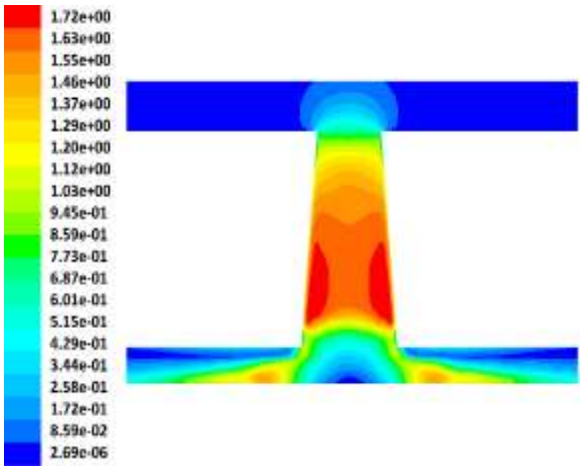

Fig.6: Output results for Mach number (nozzle 2-3 side view)

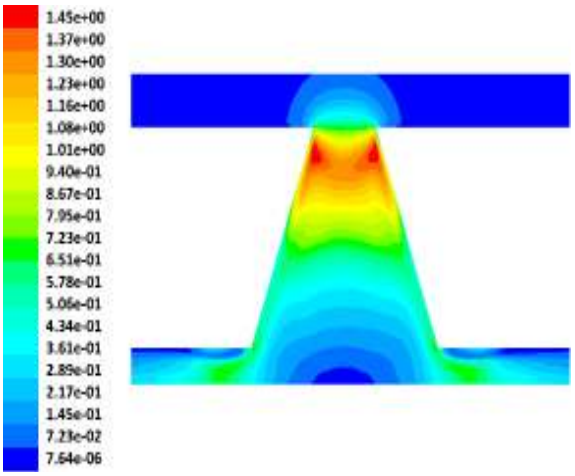

Fig.7: Output results for Mach number (nozzle 2-6 side view)

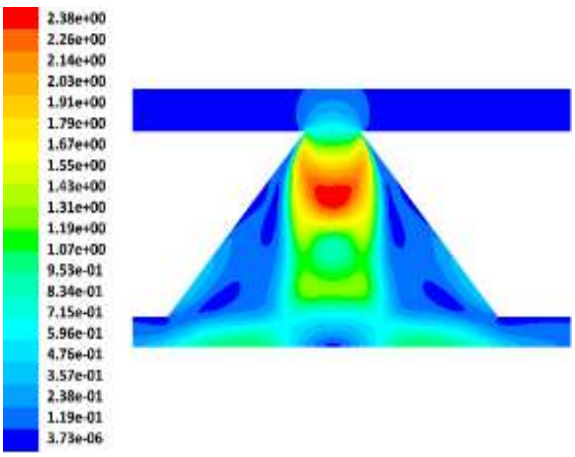

Fig.8: Output results for Mach number (nozzle 2-12 side view)

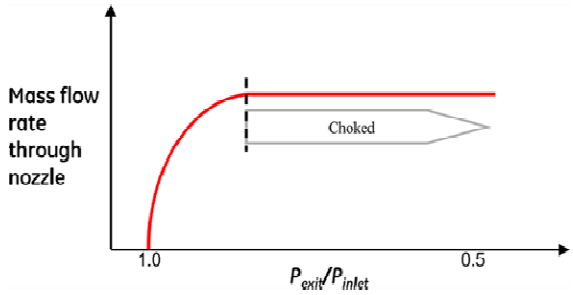

Fig.1: The mass flow rate through a nozzle at different pressure ratios (Tiwari*et al*., 2013)

stagnation area and less separation zone, the optimum shape for the nozzle will be 2 mm inlet diameter and 6 mm outlet diameter (a conical shape).

Mass-flow rate analysis: One of the fundamental concepts of physics is the conservation of mass which implies that the amount of mass remains constant in a problem domain; mass is neither created nor destroyed. The mass of an object is the volume that the object occupies times the density of the object. Figure 9 explains the relation between mass flow rate and pressure ratio. Pressure ratio is defined as the nozzle exit pressure (P_{exit}) over inlet pressure (P_{inlet}). For a fluid, the density, volume and shape of the object can all change within the domain with time.

The conservation of mass (continuity) determines that the mass flow rate $\dot{m}$ through a nozzle is constant and equal to the product of the density ρ, velocity u and flow area A:

$$\dot{m} = \rho . u . A \tag{26}$$

It is understood from the above equation that any increase in velocity for a constant density and given area, will increase the mass flow rate. However, as a result of compressibility effects in real fluid the density does not remain constant. Therefore, it is essential to take into account the effect of a change in density in higher velocities. Recalling Eq. (22) and substitute for velocity in Eq. (27), the compressible form of the mass flow rate equation is derived as:

$$\dot{m} = \rho . A . M\sqrt{\gamma RT} \tag{27}$$

Equation of state determines density as follow:

$$\rho = \frac{p}{RT} \tag{28}$$

As the flow is assumed to maintain the constant value of entropy, isentropic flow governing equations are applied (Isentropic flow occurs, if the changes in flow variables are small and gradual, e.g., the ideal gas flow through a nozzle.):

$$p = p_t (T/T_t)^{\frac{\gamma}{\gamma-1}} \tag{29}$$

$$T = \frac{T_t}{1+\frac{1}{2}(\gamma-1)M^2} \tag{30}$$

where, p_t and T_t are total pressure and total temperature respectively.

By collecting terms and substituting Eq. (28), (29) and (30) in Eq. (27), the equation for mass flow rate is derived as:

$$\dot{m} = \frac{A.p_t}{\sqrt{T_t}} . \sqrt{\frac{\gamma}{R}} . M(1 + \frac{\gamma-1}{2} . M^2)^{-\frac{\gamma+1}{2(\gamma-1)}} \tag{31}$$

The maximum flow rate occurs when the Mach number is equal to one (Bailey, 1961). This phenomenon is known as choking the flow (Bernstein, *et al*., 1967) (Fig. 9). If $M = 1$ is replaced in Eq. (32)., the value of the choked mass flow rate is determined as:

$$\dot{m} = \frac{A.p_t}{\sqrt{T_t}} . \sqrt{\frac{\gamma}{R}} . (\frac{\gamma+1}{2})^{-\frac{\gamma+1}{2(\gamma-1)}} \tag{32}$$

The mass flow rates have been calculated at cross section area where $M = 1$ using Eq. (32). For three case studies. The results are presented in Table 2.

The higher mass flow rates provide more momentum force. It is understood from the table 2, that nozzle 2-6 demonstrates the highest mass flow rate through the nozzle. These values will be used further on for validation of the numerical modelling.

EXPERIMENTAL STUDY

Laboratory tests were conducted to validate the results from the numerical study on the air-bearing unit in terms of choosing the optimum option for nozzle shape. Three different types of a nozzle (investigated in the numerical study) were tested and the optimum option was chosen for producing highest vertical force (Fig. 10).

Two sets of the test were carried out. The first set of tests were performed to determine the best nozzle type in terms of conical shape to verify numerical modelling. And the second set of tests were performed to determine the optimise a number of nozzles for the air bearing device to take desirable loads at the same inlet pressure.

The air-bearing devices used for laboratory tests were made up of aluminium in the Mechanical workshop at Anglia Ruskin University. Three types of bottom plate were made with three different types of nozzles as described below.

Tests on the air-bearing units were designed to examine the ability of each type of air-bearings in lifting designated loads. Therefore, a high precision gauge was employed to measure lift gaps at different loads and a different number of nozzles (Fig. 11). Components of the air-bearing device are shown in Fig. 12.

Table 2: Mass-flow rate calculated for three different cases

Inlet diameter (mm)	Outlet diameter (mm)	Outlet/Inlet ratio	flow rate(kg/s)
2	3	1.5	0.0313
2	6	3	0.0388
2	12	6	0.0327

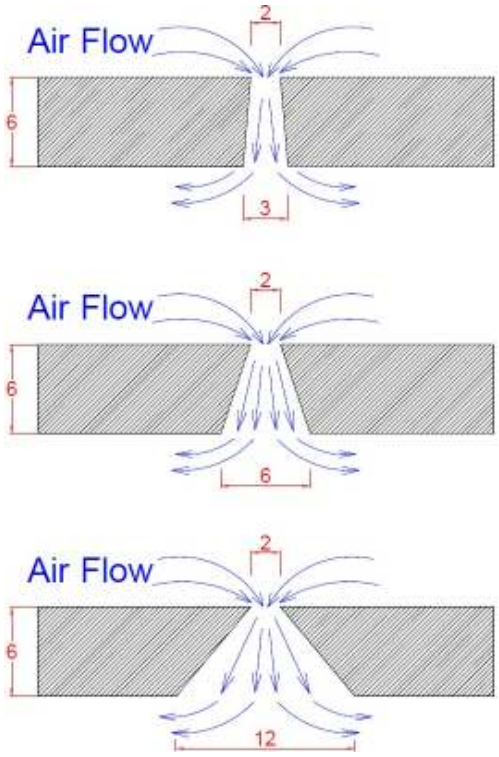

Fig. 2: Three different types of nozzle used in numerical study and laboratory tests (dimensions in mm)

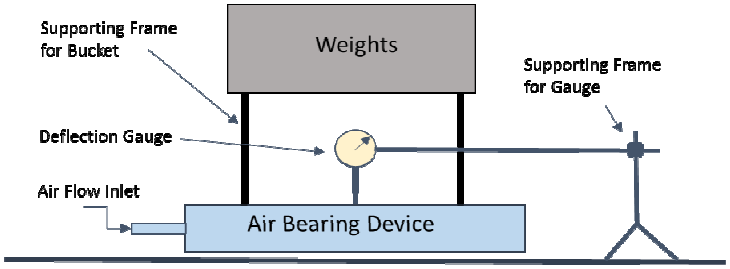

Fig.3: Test diagram

Fig.4: Air-bearing device components

Based on the capacity of the air compressor in the workshop, two different pressures were examined (5 bar and 7 bar). Inlet pressure to the chamber of an air-bearing device was adjustable with an air regulator valve.

EXPERIMENTAL RESULTS

Nozzle type: In order to validate the results from the numerical study, which shows the best performance for 2-6 mm diameter nozzle, three different nozzle types were tested in the workshop with different loading on top of the air-bearing device and recording the vertical lift read by the gauge.

Table 3 shows the performance of an air-bearing device for three different types of the nozzle

Table 3: Lifting capacity of each nozzle types investigated by experiments

	Nozzle type (D_{in}-D_{out})		
	2-3	2-6	2-12
Weight (kg)	Lift (mm)		
1.6	0.7	0.95	0.52
1.6+4	0.45	0.68	0.39
1.6+6	0.41	0.55	0.37
1.6+8	0.38	0.48	0.35
1.6+21	0.26	0.28	0.26

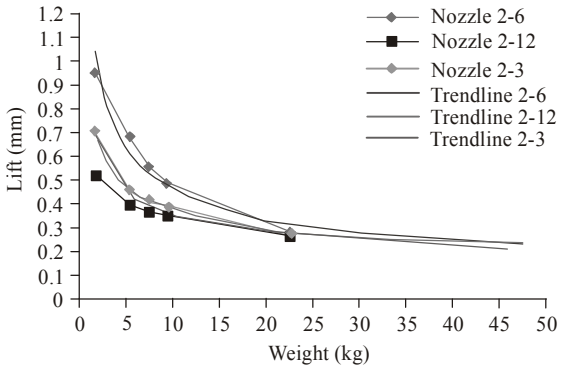

Fig.5: Lift against Weight diagram and trend lines for three different nozzles

with different loadings on 5 bar pressure. Please note that 1.6 kg corresponds to the self-weight of the device.

It is understood that the best performance belongs to the nozzle 2-6 as it provides the highest lift among others in the same pressure inlet.

Based on the drawing of trend lines on the identified points, it is possible to predict the gap when applying higher loads (Fig. 13). It should be noted that in higher loads the gaps forecasted for three nozzle shapes are almost the same, more gap lift corresponds to nozzle type 2-6.

A number of nozzles: In order to determine the optimum number of nozzles, the same procedure for loading and measuring lifts are conducted. As the nozzle 2-6 showed the best performance, this time tests are conducted just on the 2-6 type nozzle and for different numbers of the nozzle to the bottom plate of an air-bearing device to optimise the number of nozzles.

Three sets of test for this part includes (Table 4 to 6):

- Just one nozzle to the centre of bottom plate is open
- One nozzle to the centre and 6 far around
- One nozzle to the centre and 12 nozzles around

Results from these tests show the best performance in terms of lifting capacity when all 13 nozzles are open.

Figure 14 shows how the changes in the number of nozzles for air bearing affect the total gap lifts. With reference to the results from this set of tests, it is understood that the device with 13 number of nozzles has the best performance in terms of lifting the weights. However, the increase in a number of nozzles can not necessarily benefit the level of performance for this particular air bearing as the air bearing with one nozzle to the centre and six nozzles far around produces less lifting than the air bearing with just one nozzle to the centre does, in small loading conditions. This isbecause-in small loadings - the gap between the cylinder and the ground is high and it forces the air to escape from six outer nozzles easier and hence, less effectiveness in producing lift is observed. In such circumstances one single nozzle in centre produces better lift.

The another purpose of this test has been the investigation oftheeffects ofpressure onthe

Table 4: Lifts corresponding to different loadings for air bearing with one nozzle at the centre

	@ 7 bar		@ 5 bar	
Weight (kg)	Lift (mm)	Vertical stiffness (N/m)	Lift (mm)	Vertical stiffness (N/m)
1.6	0.72	21800	0.52	30184.62
3.6	0.66	53509	0.44	80263
5.6	0.61	90059	0.41	133990

Table 5: Lifts corresponding to different loadings for air bearing with one nozzle at the centre and six nozzles far around

	@ 7 bar		@ 5 bar	
Weight (kg)	Lift (mm)	Vertical stiffness (N/m)	Lift (mm)	Vertical stiffness (N/m)
1.6	1.09	14400	0.63	24914
3.6	0.63	56057	0.43	82130
5.6	0.55	99884	0.34	161577

Table 6: Lifts corresponding to different loadings for air bearing with one nozzle at the centre and 12 nozzles around

	@ 7 bar		@ 5 bar	
Weight (kg)	Lift (mm)	Vertical stiffness (N/m)	Lift (mm)	Vertical stiffness (N/m)
1.6	1.82	8624	0.95	16522
3.6	0.99	35673	0.76	46468
5.6	0.73	75255	0.68	80788

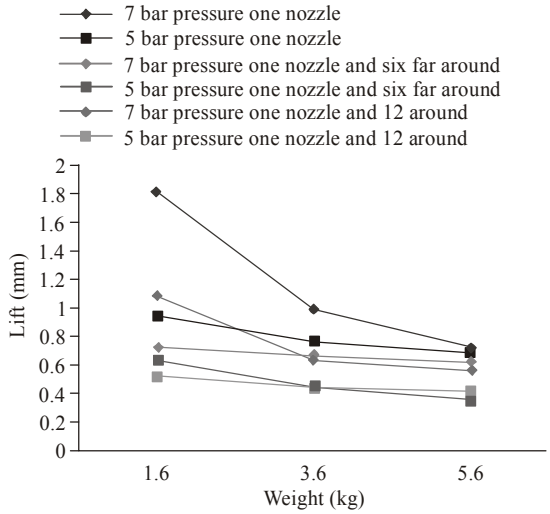

Fig.6: Lifts against weights for three different distribution of nozzles to the bottom plate

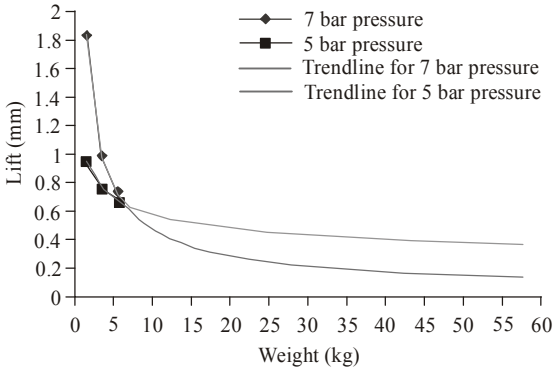

Fig.7: Different pressures on air bearing with one nozzle at the centre and 12 around

performance of air bearing. Therefore, two different pressure (5 and 7 bar) have been examined on the options for the third nozzle arrangement (one at the centre and 12 around). Figure 15 shows the trends how the lifting capacity of a specific air bearing can be different based on changes in pressure. The trend lines in this figure give an insight into choosing the desired pressure when lifting larger loads are considered. This could be due to lower gap height and negative influence of shock waves in 7 bar pressure compared to the 5 bar pressure.

VALIDATION AND COMPARISON OF RESULTS

Numerical validations: To validate the numerical study, following tests were conducted.

Grid independency: One of the most important parameters that affect the accuracy of the CFD solutions is the quality of numericalgrid.Grid dependency tests have been conducted on all cases where extra numbers of mesh did not provide any change to the solutions. It is important for the refinement to be substantial and systematic. Systematic refinement means that the grid is refined in all direction with the same ratio. The number of cells that are used for these simulations were two, three and four million that the three-million cell showed the best and robust results.

The Boundary layer is almost laminar in viscous sub-layer and fully turbulent in the log-law region. As mentioned before turbulence models are valid for fully turbulent flows, therefore semi-empirical formulas "wall functions", are used to model flow properties between the wall and log-law region. In log-law region the profile is:

$$u^+ = \frac{1}{\kappa}\ln y^+ + B = \frac{\bar{u}}{u_\tau} \quad (33)$$

where, κ is von Karman constant (κ = 0.41), u_τ is the shear velocity given by:

$$u_\tau = \sqrt{|\tau_w|/\rho} \quad (34)$$

And τ_w is the shear stress at the wall, $\bar{u}$ is the mean velocity parallel to the wall, B is an empirical constant related to the thickness of viscous sublayer and y^+ is dimensionless parameter which shows distance from the wall and is defined as:

$$y^+ = \frac{\rho u_\tau y}{\mu} \quad (35)$$

In viscous sublayer $u^+ = y^+$but in buffer layer where 5 <y^+< 30, neither law holds. In buffer layer, the effect of viscosity and turbulent are equally important.

For turbulence modelling, spatial considerations are required for grid resolution near the wall. y^+ values need to be in the log-law region; therefore, it was important to keep the y^+ values around thirty. This has been achieved with especial consideration for near wall meshes.

Results comparisons: Validation of the results from the numerical study with respect to the results from experimental observations is presented here. The parameter which can be investigated in this part is Mass-flow rate. The defined mass flow rate of the compressor, used for producing pressurised air, can be obtained from its data sheets. The actual mass flow rate of the compressor is calculated with respect to the volume rate of flow given by its manual as 1665 L/sec at 5bar pressure. Since the mass density of air is known (1.225 kg/m^3), the actual mass flow rate of the flow is simply calculated as 0.034 kg/sec. Comparing the numerically derived mass flow rates to the actual mass flow rate of the compressor shows reasonable agreement and accuracy for numerical simulations.

Table 7: Comparison of mass flow rates (kg/s)

Nozzle type	Numerical	Actual	Difference
2-3	0.0313	0.034	7.99%
2-6	0.0388	0.034	14.11%
2-12	0.0327	0.034	3.7%

Table 7 shows that there are less than 15% errors in all cases. Although the compressor data sheet does not provide mass flow rates for different pressure ratios corresponding to different nozzle geometries, it is anticipated that there will be less error in mass flow rate calculations if the data for different pressure ratio is available.

CONCLUSION

In this study design and development of the air-bearing device needed for lifting a benchmark, the structure was discussed. It was explained that how the numerical modelling can help in saving time and costs for designing a device which works with the principles of fluid's flow.

According to the results obtained from controlled laboratory tests compared to those obtained from numerical modelling, it was concluded that the best option for nozzle conical shape is 2 mm diameter inlet and 6 mm diameter outlet. This conclusion stands for the purpose of handling the heavier load at the same pressure on the proposed geometry for the air-bearing device.

Although the numerical model has its own limitations such as lack of dynamic mesh generator, it has been a useful tool for a comparative study which played a valuable role to determine the size and shape of nozzles.

Findings from physical tests were considered as validations for numerical modelling. The results from laboratory tests were further used for determination of the number of nozzles being implemented on the air-bearing device. The optimum number and positions for nozzles were then chosen.

It was also concluded that the best pressure is 5 bar in comparison to 7 bar pressure (two available stable levels of pressure can be provided in the lab) for taking larger loads.

REFERENCES

Aris, R., 1989. Vectors, Tensors and the Basic Equations of Fluid Mechanics.Dover Publications, NewYork.

Bailey, W.S., 1961. Gasparticle flow in an axisymmetric nozzle. ARS J.,31(6): 793-798.

Bernstein, A., W.H. Heiser and C.Hevenor, 1967. Compound-compressible nozzle flow. J. Appl. Mech.,34(3): 548-554.

Brennan, D., 2001. The numerical simulation of two-phase flows in settling tanks. Ph.D. Thesis, Imperial College London,London.

Clancy, L.J., 1975. Aerodynamics.Wiley,New York.

Deardorff, J.W., 1970. A numerical study of three-dimensional turbulent channel flow at large Reynolds numbers. J. Fluid Mech.,41(2): 453-480.

Eswaran, V. andS.B.Pope, 1988. Direct numerical simulations of the turbulent mixing of a passive scalar. Phys. Fluids,31(3): 506-520.

Hendriks, F., 2001. Shape optimisation of pressurised air bearings. Thesis,Rensselaer Polytechnic Institute,Hawthorne.

Jasak, H., 1996. Error Analysis and Estimation for the Finite Volume Method with Applications to Fluid Flow.Ph.D. Thesis,Imperial College of Science, Technology and Medicine,London.

Mavriplis, D.J., 1996. Mesh Generation and Adaptivity for Complex Geometries and Flows. In: Peyret,R.(Ed.),Handbook of Computational Fluid Mechanics. 2nd Edn.,Academic Press,London.

Mukai, T., 2006. Analysis of dynamic characteristics of air bearing. Nippon Steel Technical Report No. 93,Tokyo, pp: 15-17.

Powell, J.W., 1970. Design of Aerostatic Bearings.Machinery Publishing Ltd.,Brighton.

Ramezanpour, A., 2009. Authentic Optimisation Study of the Novel Compact Heat ExchanGER.1st Edn., VDM Verlag, NY.

Renn, J.C. and C.H. Hsiao, 2004. Experimental and CFD study on the mass flow-rate characteristic of gas through orifice-type restrictor in aerostatic bearings. Tribol. Int.,37(4): 309-315.

Tiwari, P., A. Steinand Y.L.Lin, 2013. Dual-solution and choked flow treatment in a streamline curvature throughflow solver. J. Turbomach., 135(4): 041004.

Wei, L. andB.Gang, 2010. Entrance effect on load capacity of orifice compensated aerostatic bearing with feeding pocket. Chinese J. Mech. Eng., 23(4).